ISSN 0036-0236, Russian Journal of Inorganic Chemistry, 2014, Vol. 59, No. 11, pp. 1298–1311. © Pleiades Publishing, Ltd., 2014.
Original Russian Text © V.G. Sevastyanov, E.P. Simonenko, A.N. Gordeev, N.P. Simonenko, A.F. Kolesnikov, E.K. Papynov, O.O. Shichalin, V.A. Avramenko, N.T. Kuznetsov, 2014, published in Zhurnal Neorganicheskoi Khimii, 2014, Vol. 59, No. 11, pp. 1542–1556.

PHYSICAL METHODS OF INVESTIGATION

HfB_2-SiC (45 vol %) Ceramic Material: Manufacture and Behavior under Long-Term Exposure to Dissociated Air Jet Flow

V. G. Sevastyanov[a], E. P. Simonenko[a, b], A. N. Gordeev[c], N. P. Simonenko[a], A. F. Kolesnikov[c], E. K. Papynov[d, e], O. O. Shichalin[d, f], V. A. Avramenko[d, e], and N. T. Kuznetsov[a]

[a] *Kurnakov Institute of General and Inorganic Chemistry, Russian Academy of Sciences, Leninskii pr. 31, Moscow, 119991 Russia*

[b] *Lomonosov Moscow State University of Fine Chemical Technologies, pr. Vernadskogo 86, Moscow, 119571, Russia*

[c] *Ishlinskii Institute for Problems in Mechanics, Russian Academy of Sciences, pr. Vernadskogo 101, block 1, Moscow, 119526 Russia*

[d] *Institute of Chemistry, Far-East Branch, Russian Academy of Sciences, pr. Stoletiya Vladivostoka 159, Vladivostok, 690022, Russia*

[e] *Far-Eastern Federal University, ul. Sukhanova 8, Vladivostok, 690950 Russia*

e-mail: ep_simonenko@mail.ru

Received May 21, 2014

Abstract—Ultra-high-temperature composite materials HfB_2-SiC containing 45 vol % SiC were prepared by spark plasma sintering. The behavior of a sample of this composition under exposure to a subsonic jet of dissociated air of a high-frequency induction plasmatron was studied; the total time was more than 30 min. Under certain test conditions, some regions of the sample were found to experience a rapid increase in temperature up to 2700°C. So, most of the surface area of the sample experienced exposure to temperatures up to 2500–2700°C for more than 15–18 min, while the rest of the surface had a temperature of 1700–1800°C during almost the entire duration of the experiment. The joint use of optical microscopy, scanning electron microscopy (with EDX analysis), X-ray powder diffraction, and X-ray computed microtomography enabled us to study the microstructure and composition of a structurally complex oxidized layer.

DOI: 10.1134/S0036023614110217

ZrB_2-SiC and HfB_2-SiC composite ceramics show promise for use in the manufacture of nose cones and sharp edges of wings in hypersonic aircrafts [1–5]. Due to the lucky combination of properties such as high melting temperatures and phase stability, high heat conductivity, and ability to form upon oxidation viscous borosilicate glasses (which serve as a barrier to air diffusion during oxidation), the aforementioned ceramic materials are capable of withstanding rapid heating and a rather long-term exposure to dissociated air flows at surface temperatures higher than 2000°C [6–9]. Most scientific publications recommend ceramic compositions comprising from 10 to 20 vol % (at most 30 vol %) silicon carbide [10–22], although materials containing more than 20 vol % SiC have also been reported [23, 24]. In order to increase mechanical strength and reduce oxidation rates, the task is to provide poreless materials at elevated temperatures (1900–2100°C). Earlier [7] we described the manufacture of HfB_2-SiC samples containing 25, 35, and 45 vol % silicon carbide using spark plasma sintering in relatively soft modes; for samples with the lowest SiC contents, we studied the behavior in a subsonic dissociated air jet.

The goal of this study was to prepare HfB_2-SiC composite materials having an increased (45 vol %) silicon carbide percentage using spark plasma sintering and to elucidate their behavior under long-term exposure to a dissociated air flow at temperatures above 2000°C.

EXPERIMENTAL

The reagents used were hafnium diboride (pure grade; particle size: 2–3 μm; aggregate size: ~20–60 μm) and silicon carbide (pure grade; average particle size: 100 μm).

The samples were manufactured on an SPS-515S Spark Plasma Sintering System setup (from Dr.Sinter-LAB™) as follows: premicronized mixtures of HfB_2 and SiC powders (where SiC percentage was 45 vol %) were placed into a graphite die, compacted, evacuated, and then sintered at a temperature lower than 1500°C under pressure and under electric pulses with an exposure time at the maximal temperature of 20 min. The resulting samples were cylinder shaped (15 mm in diameter, ~5 mm high, and ~5 g in weight).

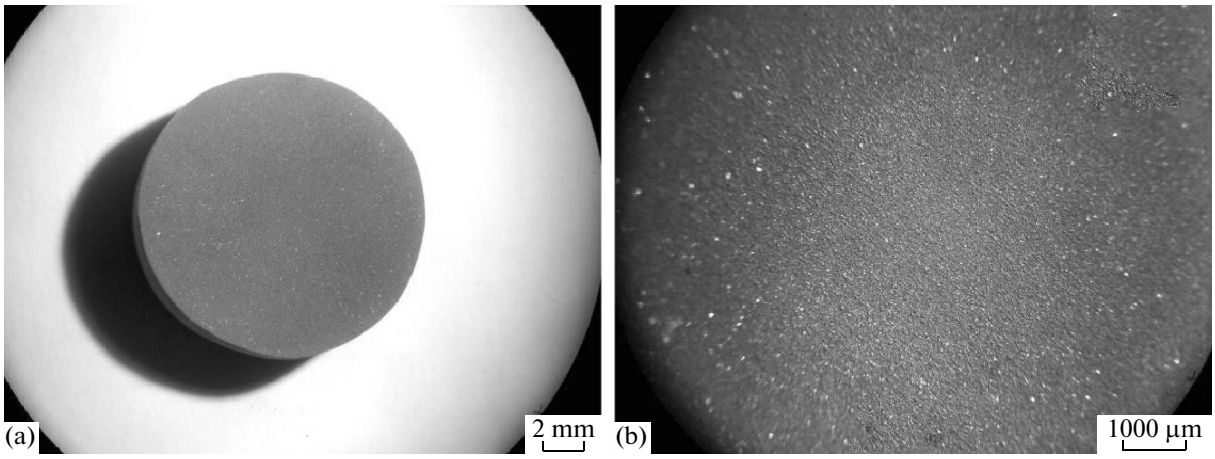

Fig. 1. (a) External appearance and (b) surface microstructure of a HfB_2-SiC (45 vol %) ceramic sample.

Surface roughness parameters were determined using a TR200 (Time Group Inc.) portable roughness tester with a baseline length of 1.25 mm.

X-ray powder diffraction studies were carried out using a Bruker D8 Advance X-ray diffraction diffractometer (CuK_α radiation, 0.02° resolution).

IR transmission spectra were recorded as Nujol mulls in KBr plates on an Infralum FT-08 IR spectrometer. IR reflection spectra were recorded using a special attachment.

The thermal behavior of products in air was studied using an SDT Q-600 integrated TGA/DSC/DTA analyzer.

Scanning electron microscopy (SEM) studies were performed on an NVision 40 (Carl Zeiss) triple-beam workstation; elemental microanalysis was carried out on an EDX Oxford Instruments energy-dispersive attachment.

X-ray computed tomography was performed on a SkyScan 1172 X-ray microtomograph with computer cluster.

Experiments, where the sample surface was exposed to a subsonic dissociated air jet, were performed on a VGU-4 100-kW high-frequency induction plasmatron [25], Institute for Problems in Mechanics, with an anode supply power of 45 to 72 kW and a pressure of 100 to 300 hPa. The surface temperature was measured with a Mikron M-770S pyrometer in the spectral ratio pyrometer mode (temperature range: 1000–3000°C; measurement spot size: ~5 mm). Temperature distribution over the front surface of the sample was determined using a Tandem VS-415U thermal imager.

RESULTS AND DISCUSSION

Characterization of Produced HfB_2-SiC Composite Materials

The HfB_2-SiC ceramic samples manufactured by spark plasma sintering contained 45 vol % silicon carbide (HfB_2-45SiC). The apparent density of these samples was 5.77 ± 0.03 g/cm^3, which corresponds to the total calculated porosity of 19.9 ± 0.5%. It should be mentioned that the HfB_2-SiC ceramic samples containing 25 and 35 vol % silicon carbide prepared earlier by similar technology had porosities of 28–32% [7]. So, we demonstrated that, the other conditions being equal, higher SiC percentages intensify sintering so that to provide a lower porosity of the sample. Surface roughness measurements showed roughness parameters close to the recommended values of less than 1–2 μm: the arithmetic mean deviation of the profile R_a defined on the baseline length of 1.25 mm was ~1.6 μm; the maximal height of the profile R_y was 6.2 μm.

The external appearance of the samples and their surface microstructure as probed by optical microscopy are displayed in Fig. 1. One cannot see large surface inhomogeneities in this figure.

The IR transmission spectra for all manufactured samples (as well as the spectra of the precursor SiC powder) featured, along with absorption bands ν(Si–C) at 800–850 cm^{-1}, a low-intensity broad absorption band with a peak at 1070–1080 cm^{-1} associated with the stretching vibrations ν(Si–O) of silicon oxide on the surface of SiC particles.

X-ray diffraction patterns of the products (Fig. 2) feature strong reflections from a hafnium diboride phase and low-intensity and broad reflections from silicon carbide.

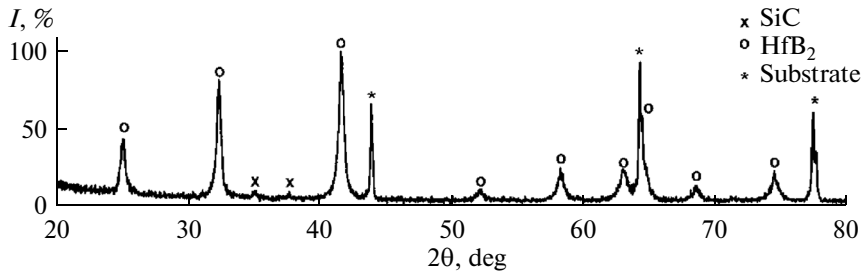

Fig. 2. X-ray diffraction pattern for our prepared HfB_2-45 vol % SiC ceramic material.

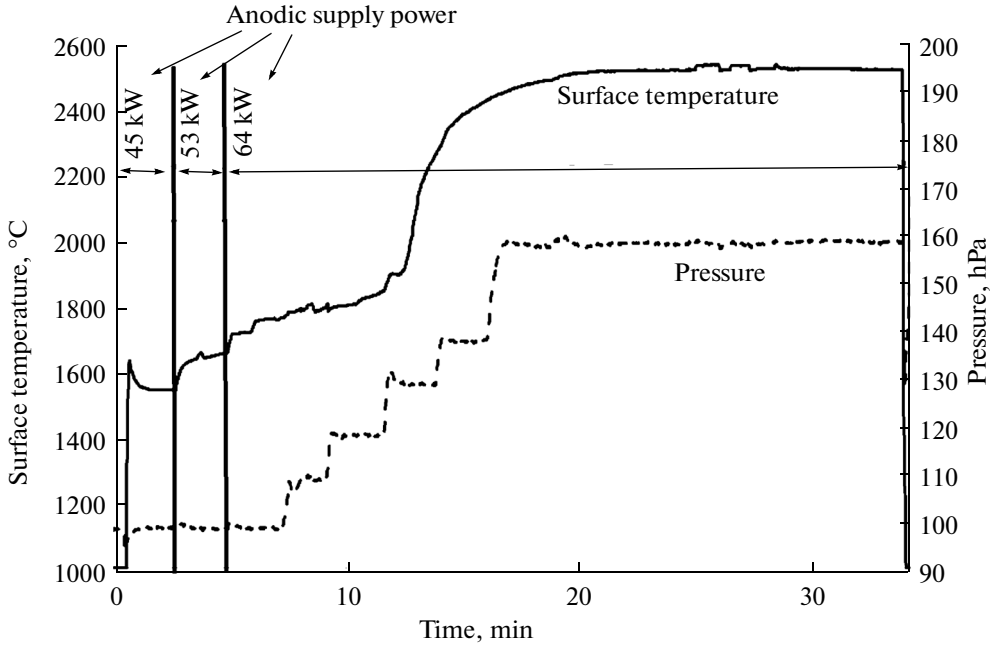

Fig. 3. Surface temperature of the sample averaged over the central region ~5 mm in diameter (measured with a Mikron M-770S pyrometer), chamber pressure, and anodic supply power in the plasmatron during exposure to a dissociated air flow.

Plasma-Chemical Study of the Behavior of HfB_2–SiC (45 vol %) Composite Material under Heating with a Dissociated Air Flow

To study the behavior of the manufactured HfB_2-45SiC composite material under heating by a subsonic dissociated air flow using a VGU-4 induction plasmatron, the sample was placed into a water-cooled copper model whose shape was identical to the ESA standard model (a flat-end cylinder with a diameter of 50 mm and a rounding edge radius of 11.5 mm). The test sample was mounted at the critical point of the water-cooled copper model by means of bundles of SiC whiskers so that to keep the sample from contact with the model. In order to reduce heat dissipation to the model, the sample was mounted so that to provide a 1.5-mm protrusion from the front surface. All experiments employed a subsonic nozzle with an the exit cross-sectional diameter of 30 mm; the distance from the sample was 30 mm, and the initial pressure in the plasmatron pressure chamber was at a level of 100 hPa.

The variation of the mean surface temperature of the HfB_2-45SiC test sample in the course of heating as determined by an M-770S Mikron pyrometer and the variation in process parameters (anodic supply power and plasmatron chamber pressure) are shown in Fig. 3. One can see from this figure that the mean surface temperature of the sample increased to ~2500°C as a result of a stepwise increase in anodic supply power and chamber pressure, after which the sample was exposed at that temperature for ~16 min (when temperature was above 2000°C, for ~20 min). It should be mentioned that, for the highest (in this experiment) anodic supply power, equal to 64 kW, and the pressure chamber of 130 hPa, the attainment of a mean surface temperature of 1880–1900°C was followed by a rapid and uncontrollable rise in temperature, which was unaf-

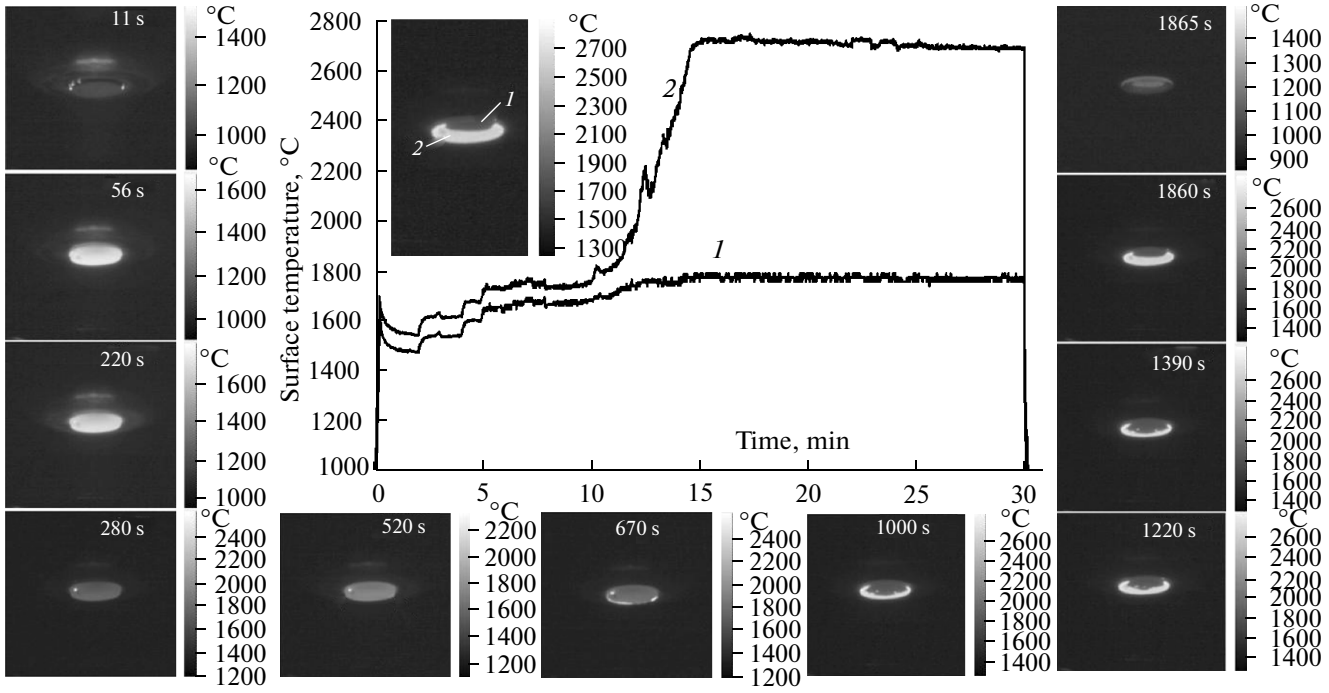

Fig. 4. Surface temperature in microregions *1* and *2* during the experiment and thermal images of the sample surface in various time intervals.

fected by subsequent changes in pressure. This provides an indirect indication that the surface at this stage became highly catalytic.

The surface-temperature variation kinetics was also studied using a Tandem VS-415U thermal imager, which records temperature distribution over the front surface. These measurements were carried out with the spectral radiation coefficient ε at the wavelength 0.9 μm, equal to 0.6. This value was selected in comparative experiments where surface temperatures were simultaneously determined for similar samples using a Tandem VS-415U thermal imager and an M770S Mikron spectral reflection pyrometer so that to provide the equality of writings of both instruments. Figure 4 displays the thermal images of the sample surface in a holder in the course of the experiment; the time elapsed from the beginning of heating is indicated on top of the corresponding image. The central inset shows the temperature variation plot for indicated regions of the sample (regions *1* and *2*). As follows from the thermal imager data, the sample is heated relatively uniformly during the initial test stages; the difference between the temperatures of regions *1* and *2* can arise from edge effects. In 4.5 min (280 s), a local overheating region having a temperature higher than 2000°C appears at the edge of the surface (mean temperature: 1550–1650°C). Cracking caused by large temperature difference does not occur. In 9 min (520 s), regions with temperatures higher than 2600°C appear at the edges of the sample; these regions are grown up in the course of the experiment, which is most prominent in 11–12 min (with the highest anodic supply power and a chamber pressure of 130 hPa).

Thus, the rise in mean surface temperature of the sample recorded with a pyrometer (Fig. 3) is due to the progressively increasing surface area where temperature is higher than 2600°C. It should be mentioned, however, that in 30 min the sample surface had yet some regions where temperature did not exceed 1700–1800°C, as indicated in Fig. 4 (region *1*).

Figure 5a displays a thermal image of the sample surface obtained in the last seconds of the experiment. The line drawn along the diameter of the sample in this image corresponds to the temperature section shown in Fig. 5b. One can see that the ~800°C temperature difference over a distance of ~1.5 mm does not induce cracking or exfoliation of the material and oxide layer under the action of a dissociated air flow.

Special attention should be paid to the last two frames in Fig. 4, which show thermal images recorded at the last second of the test and in 5 s after heating was switched off. From the curves that show the temperature schedule, one can infer that in the hottest portions of the sample (region *2*) the temperature changes by ~1680°C in 5 s, and in region *1*, by ~580°C. Moreover,

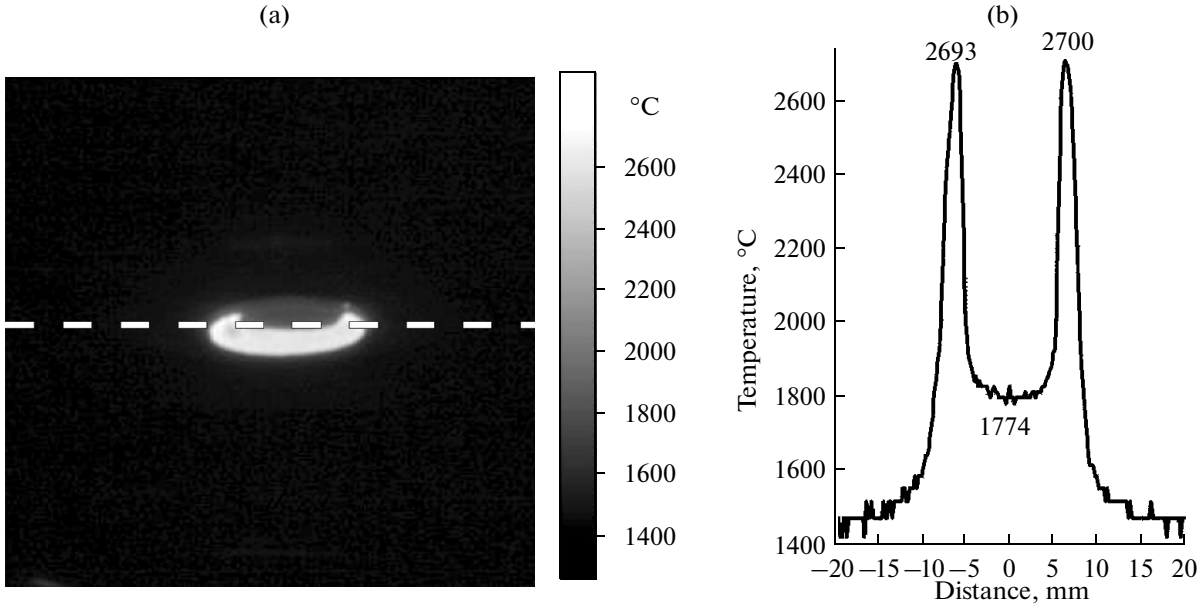

Fig. 5. (a) Thermal image of the sample surface in 31st minute of the experiment and (b) temperature along the diameter corresponding to the indicated line.

in the portion of the sample that became hotter during the experiment (region *2*), the temperature decreases at a higher rate after heating is switched off than in region *1*, which was colder during the test; that is, temperature in region *1* after 5 s of cooling is about 170°C higher than in region *2*, just as one can see in the last frame. This fact can imply a fundamental difference between the compositions of the oxidized layers in these regions of the sample, which should appreciably differ in their heat conductivities: in the maximally heated regions like region *2*, the oxidized layer should presumably consist of hafnia, which is known for its thermal barrier properties, while in "cold regions" like region *1*, the amount of low-thermal-conduction HfO_2 should be considerably lower. Thus, the newly formed hafnia (region *2*) during the experiment plays the role of a thermal barrier coating and does not allow part of the heat transferred to move into the sample bulk, which is just responsible for surface overheating, and after heating is switched off, the same low-thermal-conduction HfO_2 inhibits heat transfer from the sample bulk to the surface.

It should also be mentioned that the cracking or exfoliation of the oxidized portion of the sample does not occur during such a rapid cooling (where temperature changes by ~1650°C in 5 s), as in the earlier studies of samples containing smaller amounts of silicon carbide [7].

The external appearance of the sample after tests carried out in a water-cooled model and the surface microstructure are displayed in Fig. 6. One can see that a white porous oxidized layer has been formed in the regions in which the temperature in thermal images exceeded 2500°C during exposure to a dissociated air flow, this layer going into a denser region coated by a glass with white inclusions.

Probably, a composition saturated with hafnia (which has a low vapor pressure) was formed in high-temperature regions as a result of evaporation of silicon- and boron-containing components. On the surface of regions in which temperature was 1700–1800°C during exposure to a dissociated air flow, a borosilicate glass was formed as a result of the oxidation of the initial HfB_2-SiC material and was forced to yield to the surface due to an excessive CO pressure created under the glassy layer, through which gas diffusion is hampered: the "solid pillars–liquid roof" model [26–30].

Infrared reflection spectra (Fig. 7) verify the change experienced by the surface chemical composition of the material during the tests and the different chemical compositions of high-temperature and low-temperature regions.

The surface microstructure after the sample was exposed to a high-enthalpy plasma flux was studied in a more detailed way using scanning electron microscopy; some regions which had different temperatures during the experiment are indicated in Fig. 8. One can see that a porous oxidized layer, which typically contains both small pores (1–15 μm) and large pores (up

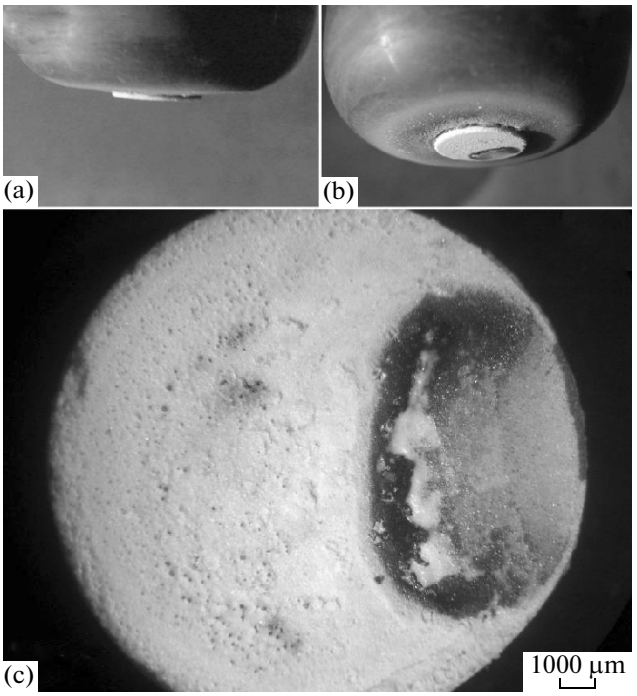

Fig. 6. (a, b) External appearance of the sample after plasma chemical exposure and (c) its surface microstructure.

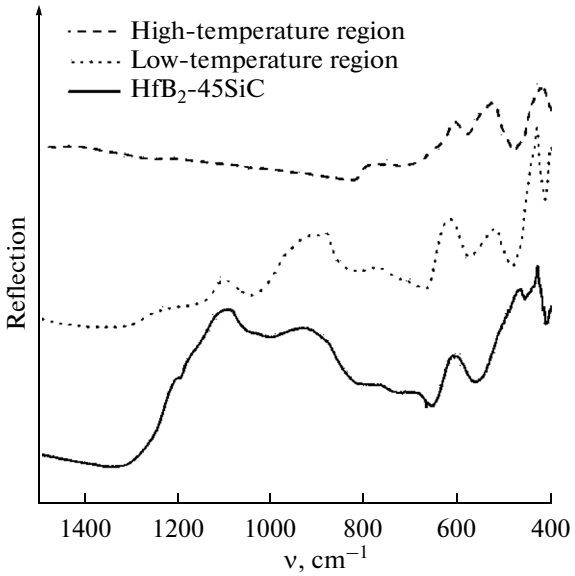

Fig. 7. IR reflection spectra from the surface of an HfB_2-45SiC sample before and after plasma chemical exposure: high-temperature and low-temperature regions.

to 100 μm), is formed in the high-temperature region (micrographs 1–3). In going from left to right toward the region that had relatively low temperatures during plasma chemical exposure, one can see in micrograph 4 how the microstructure changes from higher porosity to a dense layer. In region *5*, there is a typical glass microstructure with the absence of pores; a smooth surface is formed. In region *6*, a porous oxide framework shows itself through the glass, and in region *7*, one can see the microstructure of an edge of the sample with intrinsic medium-size porosity of up to 30 μm.

In general, such the change in microstructure along the diameter of the sample is verified by the measured roughness parameters: the arithmetic mean deviation of the profile R_a defined on the baseline length of 1.25 mm for the high-temperature region was ~6.82 μm and the maximal height of the profile R_y was 30.5 μm, while for the relatively low-temperature region $R_a = 0.84$ and $R_y = 2.83$ μm (which is smaller than the roughness of the initial HfB_2-SiC sample and is intrinsic to glassy coatings even on rather rough surfaces).

EDX surface elemental analysis was performed for the oxidized portion of the sample; the atomic percentages of silicon, hafnium and oxygen in various regions indicated in Fig. 8 are listed in Table 1. Hafnium was found to be the major component almost in all regions where a porous ceramic oxidized layer was formed (regions *1–3*); the silicon percentage was minimal (0–1.4 at %). Over the glass transition region, the hafnium percentage decreases and the silicon percentage increases in proportion; in region *5*, SiO_2 is dominantly observed with a minor (1.5 at %) hafnium percentage. The hafnium percentage systematically increases in a further approach to the edge of the sample, which is likely due to an increased temperature of this region compared to region *5* arising from the manifestation of edge effects during heating by dissociated air flows.

X-ray powder diffraction analysis was performed for the sample surface in high-temperature and low-

Table 1. Hafnium, silicon, and oxygen percentages in surface microregions of a sample after plasma chemical exposure (as probed by energy-dispersive analysis), at %

Region notation (Fig. 8)	Hf	Si	O*
1	19	0.1	56
2	17	0	57
3	17	1.4	56
4	11	6	60
5	1.5	19	63
6	10	11	58
7	12	8	54

* An estimate.

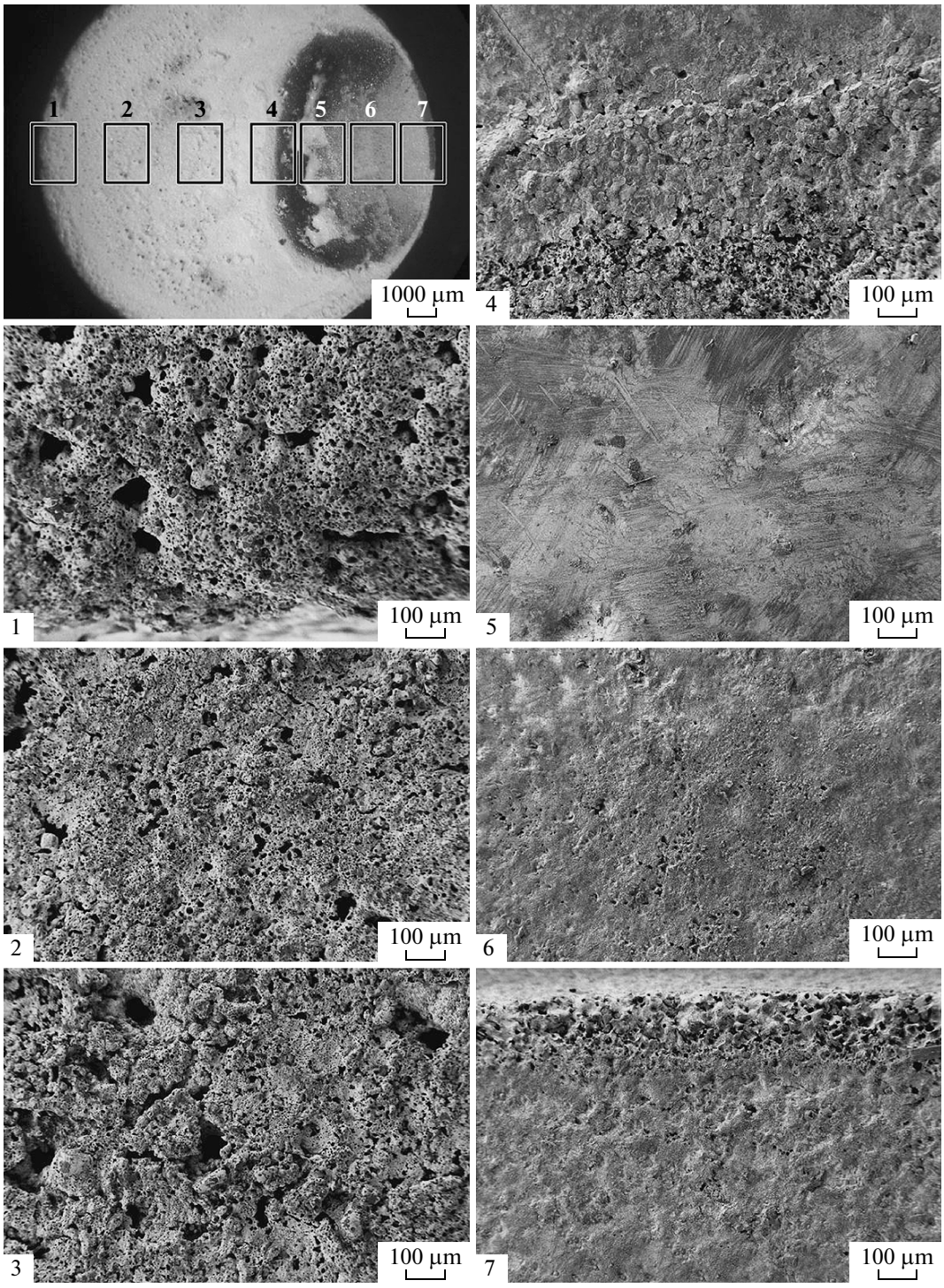

Fig. 8. Microstructure observed in selected surface areas of a sample after long-term heating in dissociated air flows.

temperature regions (~5 × 5 mm); the relevant X-ray diffraction patterns are displayed in Fig. 9.

Both X-ray diffraction patterns feature reflections from an impurity hafnium diboride phase, which was likely introduced during sample preparation for the X-ray diffraction experiment; this phase is absent on the sample surface after the tests, since optical microscopy verifies the absence of grey particles. In region *2* (which experienced exposure to higher temperatures of ~2500–2680°C), a monoclinic hafnium diboride

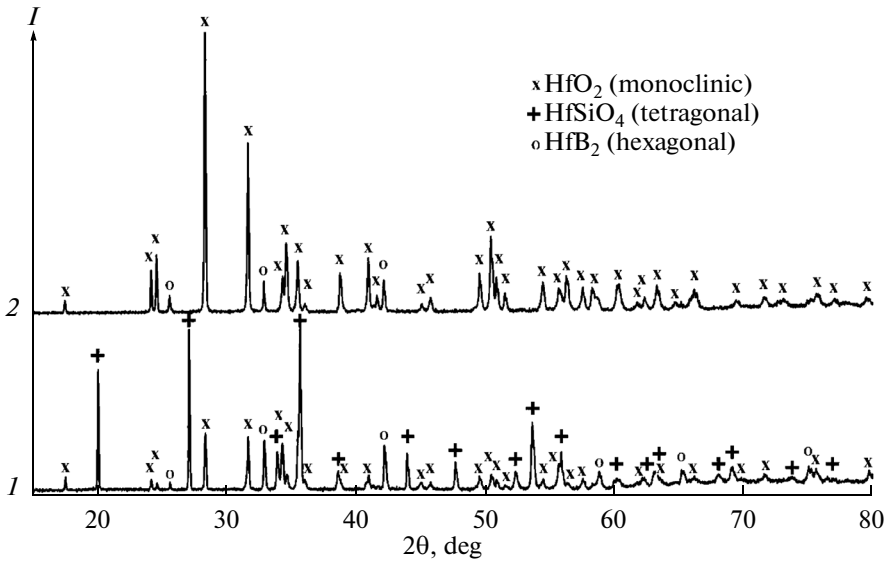

Fig. 9. X-ray diffraction patterns recorded from the surface of a sample after exposure to dissociated air flow: region *1* (lower panel) and region *2* (upper panel).

phase is present on the surface. For region *1* (where temperature was 1700–1800°C during a long time in the course of the plasma chemical test), the major phase (~60%) is hafnium silicate $HfSiO_4$ mixed with monoclinic HfO_2. Evidently, having regard to the HfO_2-SiO_2 phase diagram [31], we may imply that such conditions (time, temperature, and concentrations) were generated at 1750 ± 50°C that favored the predominant vaporization of boron and silicon oxides from the melt and subsequent crystallization of hafnon (probably with an admixture of monoclinic HfO_2) in pores of refractory hafnia.

A more detailed study of the bulk oxidation of a sample involved the examination of a polished section by optical microscopy (Fig. 10) and scanning electron microscopy (Fig. 11).

One can see from Fig. 10 that the oxidized areas in high-temperature and low-temperature regions have appreciably differing thicknesses. For a region exposed to temperatures of up to 2700°C, the multilayer oxidized region, whose surface composition is dominated by HfO_2, has a thickness of ~500–600 μm. For a region heated to 1700–1800°C, the oxidized layer thickness is within 100 μm. In addition, on the optical micrograph one can recognize a deeper lying layer 600–800 μm thick, which is darker than the bulk and has another microstructure (the boundary of this layer is indicated by a dashed line).

The regions indicated in Fig. 10 were studied by SEM (Figs. 11, 12). One can see in Fig. 11 that the overall thickness of the oxidized layer decreases with lowering temperature that was attained on the sample surface during exposure to a dissociated air flow. On the whole, few layers can be recognized in the oxidized region, as demonstrated in our earlier studies, for example in [7], and noticed by most of our colleagues. In the region experienced exposure to ~2500–2700°C (Figs. 11.1, 11.2, 12.6), a porous layer ~300–400 μm thick is formed on the surface, likely consisting mostly

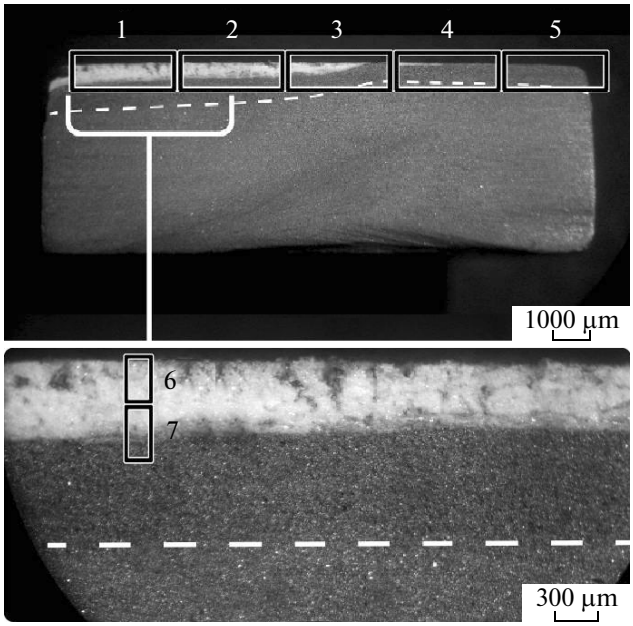

Fig. 10. Structure of a polished section of an HfB_2-45SiC sample after long-term exposure to a dissociated air flow.

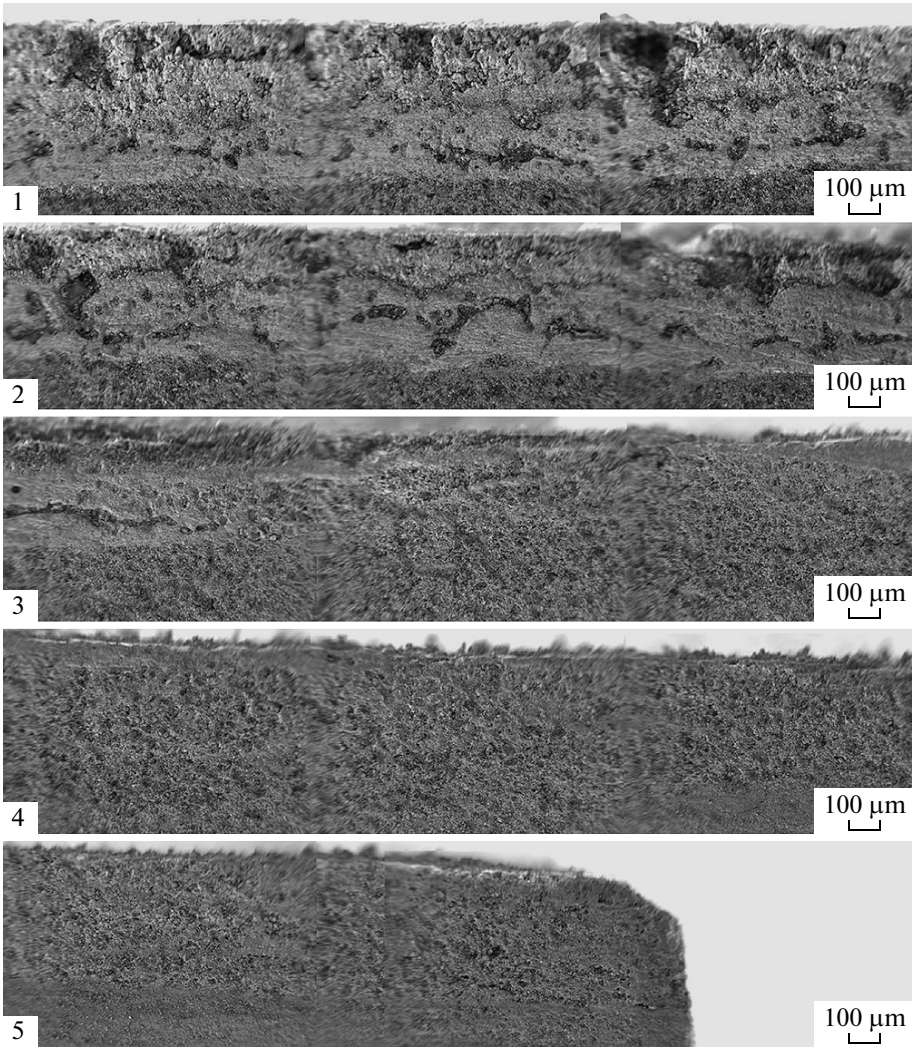

Fig. 11. Microstructure (as observed by SEM) in selected areas of the near-surface oxidized layer indicated in Fig. 10. Scans over the surface.

of HfO_2 and having pore sizes of up to 50–100 μm. Underneath there is the denser layer with horizontally oriented extended pores in which borosilicate glass (which performs as an oxygen diffusion barrier) was concentrated during the plasma chemical experiments. In still deeper layers, a layer having another microstructure was formed, most likely in the course of the active oxidation of silicon carbide (to form gaseous CO and SiO because a reduced oxygen concentration). The oxygen, silicon, and hafnium distribution maps shown in Fig. 13 make it possible to estimate the thicknesses of these layers more accurately. One can see that hafnium and oxygen are mostly concentrated on the surface with some (small) silicon percentage (the layer thickness is ~300–400 μm). In a deeper and denser layer ~200–300 μm thick, one can see a reduced hafnium percentage and increased silicon and oxygen percentages. This second layer is underlain by a region where hafnium is concentrated, which is depleted in silicon and has an insignificant oxygen percentage. The thickness of this region is ~200–300 μm. The SiC-depleted region is likely to appear in optical micrographs and is part of the darker layer with another microstructure (600–800 μm thick).

EDX analysis was used to quantify how the element percentage ratios change in going along the polished section into the depth of the material (Fig. 14, Table 2).

One can see that the silicon percentage is minimal (1 at %) at a distance of ~200–300 μm from the surface (spectra *1* and *2*), but at a depth of 400–450 μm this percentage increases ninefold with a simultaneous small decrease in hafnium percentage (spectrum *3*). Immediately at the lower boundary of the low-electrical-conductivity oxidized layer at a distance of ~550 μm

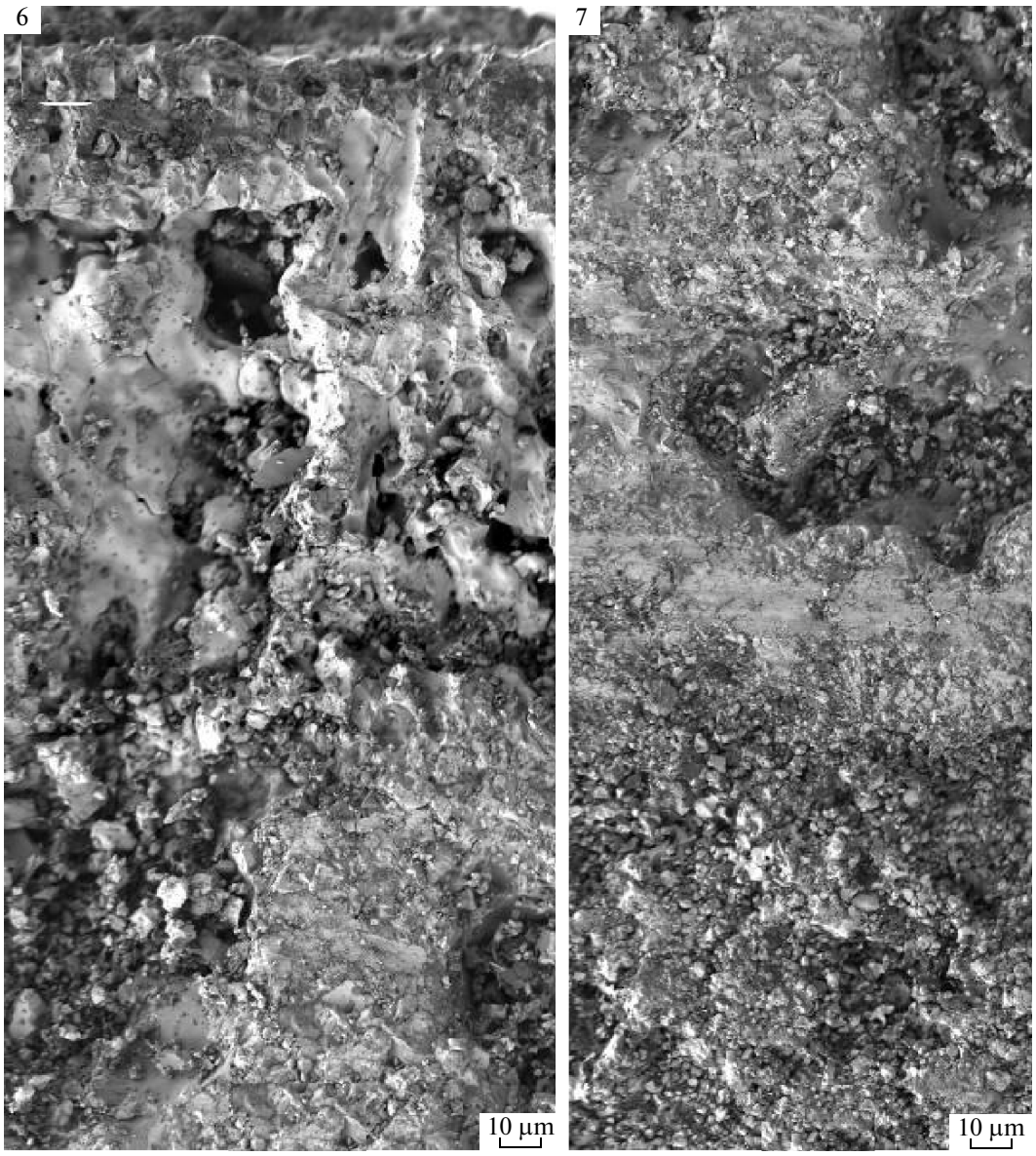

Fig. 12. Microstructure (as observed by SEM) in selected areas of the near-surface oxidized layer indicated in Fig. 10. Scans into the depth of the region that experienced exposure to the temperatures in the course of the plasma chemical experiment.

from the surface (spectrum *4*), there is no silicon at all (as probed by EDX), but there is a reduced oxygen percentage and a high hafnium percentage. This is likely to prove that the dense borosilicate layer, which is at a distance of 400–550 μm from the surface, is underlain by a partially oxidized hafnium diboride layer. And ~50 μm lower (spectrum *5*), immediately under this layer, the oxygen concentration decreases to zero; EDX here detects only hafnium (likely in hafnium diboride). Spectra *6* and *7* (which characterize regions lying at a distance of 650–750 μm from the surface) show a gradual increase in silicon percentage to reach (in deeper layers at a distance of ~800–850 μm) the concentration intrinsic to the initial HfB_2-SiC sample.

Returning to Figs. 10 and 11, we have to analyze the microstructure in the near-surface region of the sample which experienced exposure to lower temperatures (1700–1800°C) during the plasma chemical experiment; these are the vicinities of region *4* (Fig. 10). Figure 15 displays oxygen, silicon, and hafnium distributions across the polished section. One can see an oxide layer of an insignificant thickness (<100 μm) concentrated immediately on the surface; this layer likely consists of melt-crystallized borosilicate glass, hafnon, and hafnium oxide (resulting from HfB_2 oxidation). In

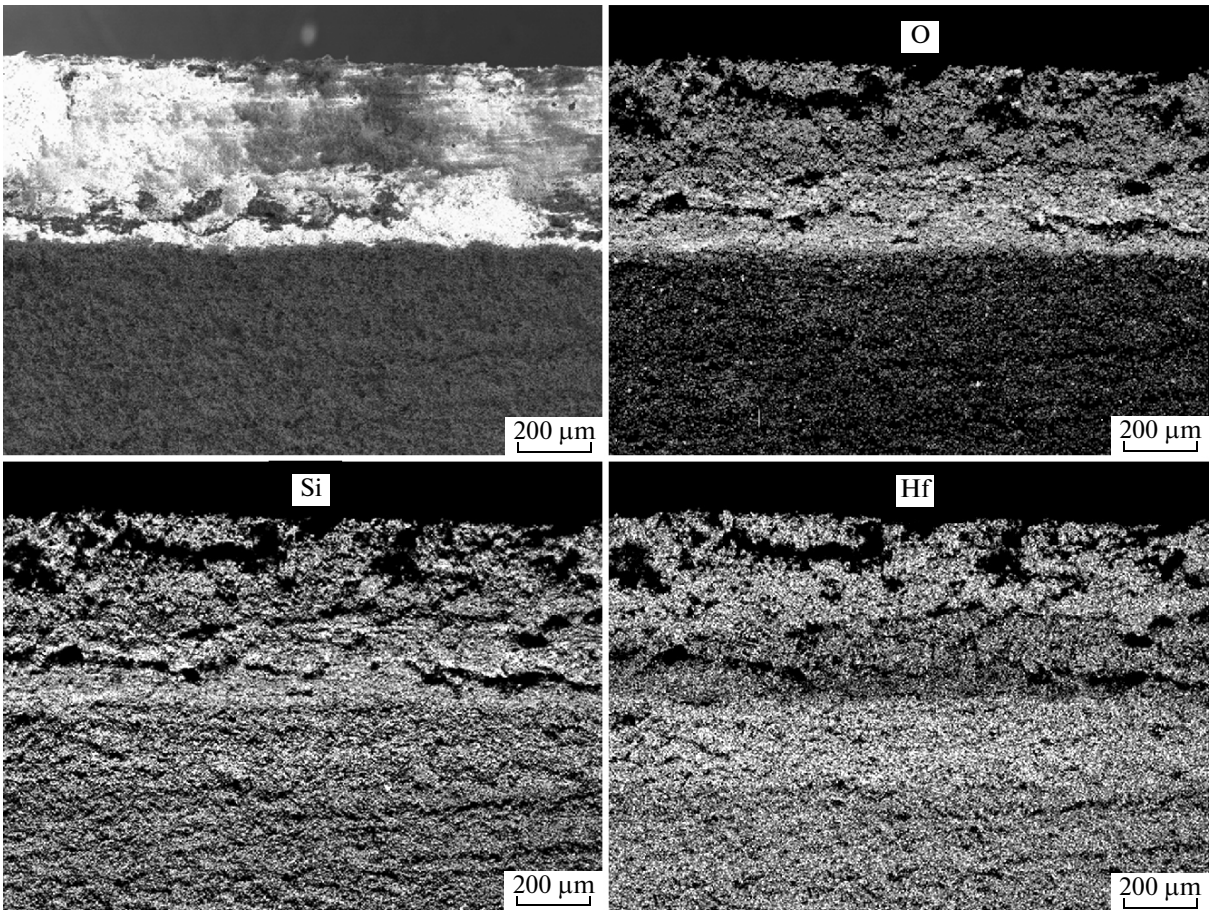

Fig. 13. Oxygen, silicon, and hafnium distribution maps in the near-surface regions of a sample that experienced exposure to a dissociated air flow (surface temperature: ~2500–2700°C).

deeper layers, one can see very low oxygen percentage, relatively low silicon percentage, and concentrated hafnium. This layer, which has a thickness of 300–400 μm, is likely to consist of partially oxidized HfB_2 with a reduced percentage of SiC, which is also involved in active oxidation (to form mainly gaseous CO and SiO rather than liquid SiO_2).

Table 2. Hafnium, silicon, and oxygen percentages in microregions (a high-temperature region) in a polished section of a sample after plasma chemical exposure (as probed by energy-dispersive analysis), at %

Region notation (Fig. 14)	Hf	Si	O*
1	27	1	72
2	29	1	70
3	25	9	66
4	52	0	48
5	100	0	0
6	98	2	0
7	92	8	0

* Estimate.

The more detailed structural analysis directly of the oxidized region with the use of EDX analysis showed that, despite an insignificant thickness, this layer has a complex structure (Fig. 16, Table 3). On the surface, there is a rather inhomogeneous layer, which contains both oxidized silicon and hafnium. At a depth of ~50 μm, there is a dense layer, also about 50 μm thick, in which hafnium percentage is very low; probably, this is the region where borosilicate glass is concentrated in pores of the HfO_2-based framework.

Further (spectrum *3*), while hafnium percentage increases appreciably, the silicon percentage is reduced to a very considerable degree and the oxygen percentage is reduced even more noticeably. This region can likely be recognized as a low-oxidized hafnium diboride layer from which some silicon is removed due to the formation of silicon monoxide and carbon monoxide (and some SiO is oxidized at the lower boundary of the borosilicate glass through which oxygen diffuses).

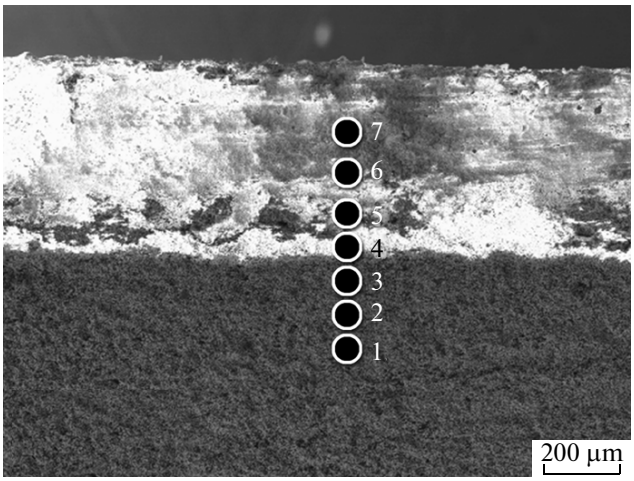

Fig. 14. Microstructure of region *1* (Fig. 10) with regions indicated for energy-dispersive microanalysis to be performed.

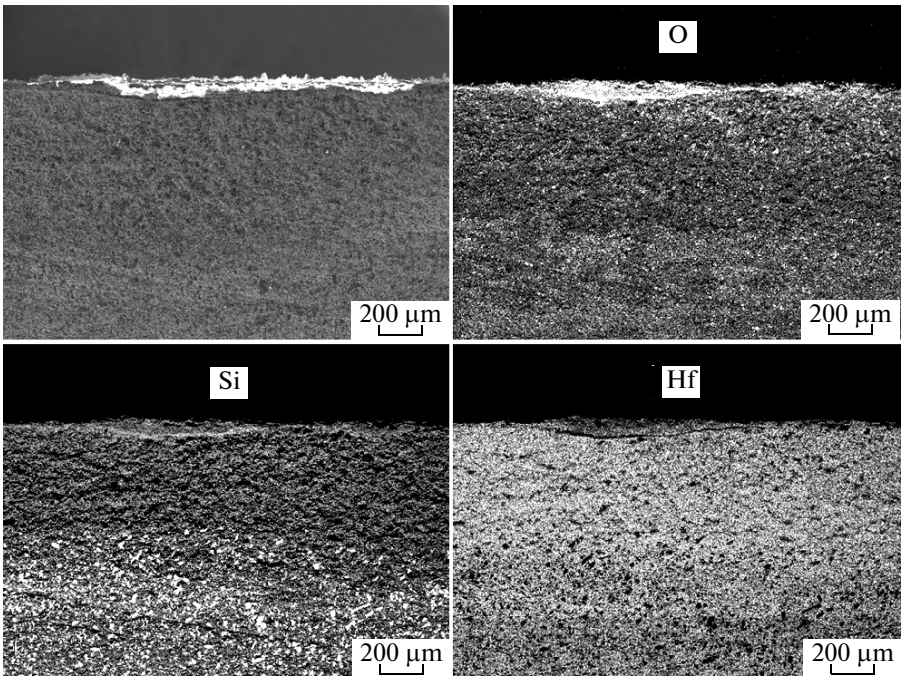

Fig. 15. Oxygen, silicon, and hafnium distribution maps in the near-surface regions of a sample that experienced exposure to a dissociated air flow (surface temperature: ~1700–1800°C).

Combining data gained by optical and electronic microscopy, we can infer that the thickness, microstructure, and elemental and phase composition of the oxidized region are appreciably differentiated depending on the temperature conditions of exposure of the HfB_2-45SiC sample. Micrographs do not show that the oxide portion of the oxidized region is exfoliated from the region with reduced SiC percentage, despite the appreciable differences between the thermomechanical properties of the HfB_2, SiC, $HfSiO_4$, and HfO_2 components. The total thickness of the oxidized layers for the region that experienced long-term exposure to temperatures of ~2500–2700°C, including the silicon carbide-depleted region, was 800–850 μm (up to 1500 μm as probed by optical microscopy), and for the region heated to ~1700–1800°C, the total thick-

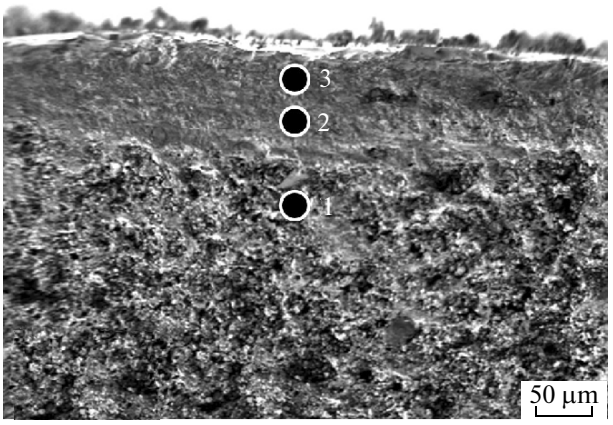

Fig. 16. Microstructure of region *4* (Fig. 10) with regions indicated for energy-dispersive microanalysis to be performed.

Fig. 17. Flat section along the diameter of an HfB_2-45SiC sample after plasma chemical exposure (as probed by X-ray computed microtomography).

ness was 400–500 μm. The total thickness of the oxidized layers, except for the silicon carbide-depleted region, is ~500–700 μm for the high-temperature region and within 100 μm for the low-temperature region.

Table 3. Hafnium, silicon, and oxygen percentages in microregions (a low-temperature region) in a polished section of a sample after plasma chemical exposure (as probed by energy-dispersive analysis), at %

Region notation (Fig. 16)	Hf	Si	O*
1	19	31	48
2	0.5	19	78
3	26	15	38

* Estimate.

X-ray computed microtomography also verified the absence of cracks and significant defects in the bulk material and at the boundary of the oxidized region. Figure 17 displays the X-ray diffraction section along the diameter of the sample after exposure to a dissociated air flow.

CONCLUSIONS

We employed an advanced method of spark plasma sintering to manufacture ultra-high-temperature composite materials HfB_2–SiC having high bulk silicon carbide percentage (45%) and the tailored porosity of ~20%. We have not observed significant defects on the sample surfaces; the arithmetic mean deviation of the profile derived from surface roughness was ~1.6 μm. The elemental and phase composition of the materials have been studied.

The behavior of an HfB_2-45SiC sample under exposure to a subsonic jet of dissociated air has been studied in a high-frequency induction plasmatron. We have found using a pyrometer that the surface temperature of the sample changes depending on the anodic supply power and on the pressure in the plasmatron chamber, but once the average temperature measured by a pyrometer reaches 1800–1900°C, the temperature rapidly rises to acquire values far exceeding 2000°C. The use of a thermal imager enabled us to determine that a sample is heated relatively uniformly at the initial test stages (1500–1800°C depending on the power and pressure); in 9 min, regions where temperature exceeds 2500°C appear at the edges of the sample to slowly grow up in the course of the experiment thereby increasing the mean surface temperature of the sample. It follows that some surface regions of the sample experienced exposure to temperatures of 2500–2700°C for periods of time longer than 15–18 min, and some regions had temperatures of 1700–1800°C almost during the entire experiment. The overall test time of the sample was longer than 30 min. Neither degradation nor exfoliation of the material or oxidized layer was observed; the weight loss of the sample as a result of exposure to a dissociated air flow was 1.5%.

We have noticed that, although temperature lowered as a result of stopped heating very rapidly (the high-temperature regions were cooled by ~1680°C in 5 s and the low-temperature regions by ~580°C in the same period), neither cracking nor any defects appeared. The oxidized surface of the sample had lower thermal conductivity in the regions that had been heated to 2500–2700°C in the course of the experiment than in the regions that had been heated to 1700–1800°C, and this was manifested in the character of thermal images obtained upon cooling. IR reflection spectra confirmed that the chemical composition on the surface of the material changes in the course of tests and the chemical compositions in the high-temperature region and low-temperature region

are different. X-ray powder diffraction showed an oxidized layer based on monoclinic HfO_2 to form on the surface of the sample in the region exposed to temperatures of 2500–2700°C, while in the region with lower temperatures, hafnon (~60%) crystallized from melt and HfO_2 (monoclinic) was present.

We have discovered using optical and electronic microscopy that the oxidized layer thickness also appreciably depends on the surface temperature. In the region experienced exposure to temperatures higher than 2000°C, a rather thick multilayered system is formed. Hafnia is concentrated mainly on the surface as a porous layer having a thickness of about 300–400 μm; below, there is a region with increased borosilicate glass percentage (200–300 μm thick), and in deeper layers, there is a region of insignificantly oxidized HfB_2 which is depleted in silicon carbide because of its active oxidation, also 200–300 μm thick. In the region that experienced exposure to appreciably lower temperatures (1700–1800°C), there is also a hafnium-enriched oxidized region with a complex microstructure (a noticeable structural inhomogeneity is likely to arise from the formation of a HfO_2–$HfSiO_4$ multiphase system). Borosilicate glass (which functions as a barrier to in-depth oxygen diffusion) is likely to be concentrated below, and in deeper layers there is a region where SiC-depleted low-oxidized hafnium diboride exists. The overall thickness of this multilayer system is ~400–500 μm, where the oxidized portion accounts for at most 100 μm.

X-ray computed microtomography verified the inference made from optical microscopy and SEM about the absence of cracks and defects in the bulk of the sample or in the near-surface layer, in spite of considerable temperature differences experienced by the sample.

Our studies support the potential of the materials having high silicon carbide percentages (45 vol %), which were manufactured using spark plasma sintering, for use under exposure to heating in a dissociated air flow at ultrahigh temperatures.

ACKNOWLEDGMENTS

This study was supported by a grant for young scientists of the President of the Russian Federation through (MK-1435.2013.3) and the Russian Foundation for Basic Research (project no. 13-03-12206-ofi_m).

REFERENCES

1. E. P. Simonenko, D. V. Sevast'yanov, N. P. Simonenko, et al., Russ. J. Inorg. Chem. **58**, 1669 (2013).
2. M. M. Opeka, I. G. Talmy, and J. A. Zaykoski, J. Mater. Sci. **39**, 5887 (2004).
3. F. Monteverde and R. Savino, J. Am. Ceram. Soc. **95**, 2282 (2012).
4. T. H. Squire and J. Marschall, J. Eur. Ceram. Soc. **30**, 2239 (2010).
5. W. G. Fahrenholtz and G. E. Hilmas, Int. Mater. Rev. **57** (1), 61 (2012).
6. J. Marschall, D. A. Pejakovi, W. G. Fahrenholtz, et al., J. Thermophys. Heat Transfer **26**, 559 (2012).
7. V. G. Sevast'yanov, E. P. Simonenko, A.N. Gordeev, et al., Russ. J. Inorg. Chem. **58**, 1269 (2013).
8. M. Gasch, D. Ellerby, E. Irby, et al., J. Mater. Sci. **39**, 5925 (2004).
9. X. Jin, R. He, X. Zhang, et al., J. Alloys Compd. **566**, 125 (2013).
10. F. Monteverde, R. Savino, and M. Fumo, Corros. Sci. **53**, 922 (2011).
11. J. B. Berkowitz-Mattuck, Technical Report ASDTDR-62-203, AFML, WPAFB, OH (1962/1963).
12. F. Monteverde, R. Savino, M. Fumo, et al., J. Eur. Ceram. Soc. **30**, 2313 (2010).
13. M. Gasch and S. Johnson, J. Eur. Ceram. Soc. **30**, 2337 (2010).
14. D. Sciti and L. Silvestroni, J. Eur. Ceram. Soc. **32**, 1933 (2012).
15. D. Sciti, R. Savino, and L. Silvestroni, J. Eur. Ceram. Soc. **32**, 1837 (2012).
16. J. Zou, G.-J. Zhang, C.-F. Hub, et al., J. Eur. Ceram. Soc. **32**, 2519 (2012).
17. L. Silvestroni and D. Sciti, J. Eur. Ceram. Soc. **33**, 403 (2013).
18. M. W. Bird, R. P. Aunea, F. Yu, et al., J. Eur. Ceram. Soc. **33**, 2407 (2013).
19. J. Zou, G.-J. Zhang, J. Vleugels, and O. Van der Biestba, J. Eur. Ceram. Soc. **33**, 1609 (2013).
20. S. Gangireddy, J. W. Halloran, and Z. N. Wing, J. Eur. Ceram. Soc. **33**, 2901 (2013).
21. W. Tan, C. A. Petorak, and R. W. Trice, J. Eur. Ceram. Soc. **34**, 1 (2014).
22. C. Carney, A. Paul, S. Venugopal, et al., J. Eur. Ceram. Soc. **34**, 1045 (2014).
23. M. Tului, B. Giambi, S. Lionetti, et al., Surf. Coat. Technol. **207**, 182 (2012).
24. P. A. Williams, R. Sakidj, J. H. Perepezko, and P. Ritt, J. Eur. Ceram. Soc. **32**, 3875 (2012).
25. A. N. Gordeev and A. F. Kolesnikov, *Topics of Mechanics: Physicochemical Mechanics of Liquids and Gases* (Nauka, Moscow, 2010) [in Russian].
26. J. Li, T. J. Lenosky, C. J. Först, et al., J. Am. Ceram. Soc. **91**, 1475 (2008).
27. T. A. Parthasarathy, R. A. Rapp, M. Opeka, et al., J. Am. Ceram. Soc. **95**, 338 (2012).
28. D. Gao, Y. Zhang, and J. Fu, Corros. Sci. **52**, 3297 (2010).
29. W. G. Fahrenholtz, J. Am. Ceram. Soc. **90**, 143 (2007).
30. T. A. Parthasarathy, M. D. Petry, M. K. Cinibulk, et al., J. Am. Ceram. Soc. **96**, 907 (2013).
31. V. N. Parfenenkov, R. G. Grebenshchikov, and N. A. Toropov, Dokl. Akad. Nauk SSSR **185**, 840 (1969).

Translated by O. Fedorova